Superlattice-induced minigaps in graphene band structure due to underlying one-dimensional nanostructuration

A. Celis,[1] M. N. Nair,[2,1] M. Sicot,[3] F. Nicolas,[2] S. Kubsky,[2] D. Malterre,[3] A. Taleb-Ibrahimi,[2] and A. Tejeda[1,2,*]

[1]*Laboratoire de Physique des Solides, CNRS, Université Paris–Sud, Université Paris–Saclay, 91405 Orsay, France*

[2]*Synchrotron SOLEIL, Saint-Aubin, 91192 Gif-sur-Yvette, France*

[3]*Institut Jean Lamour, UMR 7198 CNRS, Université de Lorraine, 54506 Vandoeuvre lès Nancy, France*

(Received 22 December 2017; revised manuscript received 12 April 2018; published 8 May 2018)

We have studied the influence of one-dimensional periodic nanostructured substrates on graphene band structure. One-monolayer-thick graphene is extremely sensitive to periodic terrace arrays, as demonstrated on two different nanostructured substrates, namely Ir(332) and multivicinal curved Pt(111). Photoemission shows the presence of minigaps related to the spatial periodicity. The potential barrier strength of the one-dimensional periodic nanostructuration can be tailored with the step-edge type and the nature of the substrate. The minigap opening further demonstrates the presence of backward scattered electronic waves on the surface and the absence of Klein tunneling on the substrate, probably due to the fast variation of the potential, of a spatial extent of the order of the lattice parameter of graphene.

DOI: 10.1103/PhysRevB.97.195410

I. INTRODUCTION

Quantum confinement and structural superperiodicities are well-known procedures to tailor electronic properties in massive fermion systems [1–3]. Superperiodic potentials of spatial period L can lead to the apparition of band replicas (umklapps), displaced in the reciprocal space by $G = 2\pi/L$. At the intersection between the original band and the replicas (i.e., at the Brillouin zone edge of the new periodicity), minigaps open up due to the backscattering of electrons at the potential barrier [4–6]. In graphene, the situation can be different if Klein tunneling protects the backscattering [7]. In this situation, when the barrier is sharper than the electron wavelength, electrons do not backscatter at normal incidence from the potential barrier, as experimentally demonstrated [8,9]. This particularity of Dirac electrons has been studied in slowly varying superperiodic potentials [10–12], where the spatial variation of the potential is much smaller than the intercarbon distance, in order to avoid intervalley scattering. In this situation, therefore, the chirality of graphene prevents the band-gap opening [10,11], although new Dirac points associated with the periodicity are observed.

The influence of electron backscattering in graphene under a superperiodic potential can be studied by graphene growth on nanostructured substrates. The ultimate monolayer thickness of graphene makes graphene extremely sensitive to underlying or overlying nanostructuration. It has been observed that graphene feels a two-dimensional potential when it is grown on noble metal [13,14], directly attached to the SiC (buffer layer) [15–17] or deposited on a BN substrate [10,18], because of the stacking-induced moiré pattern. One-dimensional structurations rely on corrugations [19], graphene suspension on nanotrenches [20], e-beam induced nanostructures [21], and growth on different vicinal surfaces [22–25]. Scanning tunneling spectroscopy has allowed to observe in some cases the appearance of the superlattice Dirac points [18,19,22,26], observed as extra dips in the density of states. On two-dimensional moirés, minigaps have even been observed directly in the band structure [14,27]. On one-dimensional systems, and despite all the interest that these systems have evoked [10–12,28–32], no gap has ever been observed in direct measurements of the band structure [23,24,33]. In this paper, we focus precisely on graphene grown on one-dimensional nanostructured vicinal surfaces. We successfully identify minigap openings at the crossing of the Dirac cones along the superperiodicity direction, making explicit the partial confinement of the electronic waves and the absence of Klein tunneling. We also quantify the strength of the potential barrier when graphene grows on different periodic nanostructures.

II. EXPERIMENTAL DETAILS

The experiments were carried out in three different ultrahigh-vacuum chambers equipped with low-energy electron diffraction (LEED). We measured at CASSIOPEE beamline and at the Surface Laboratory of SOLEIL for high-resolution angle-resolved photoemission spectroscopy (ARPES) with a spot size of the order of 50 microns, and room-temperature scanning tunneling microscopy (STM), respectively, and we performed low-temperature STM measurements at the Institut Jean Lamour setup (77 K). Photoemission experiments were performed at a photon energy of 36 eV and 77 K. The substrates were Ir(332) from Surface Preparation Laboratory and a curved multivicinal Pt(111) crystal from BihurCrystal. The pristine Ir(332) surface is composed of 1.25 nm width steps that extend along the $[10\bar{1}]$ direction. The macroscopic normal of multivicinal Pt(111) ranges from 0° on the (111) surface up to 16° toward the $[11\bar{2}]$ and $[\bar{1}\bar{1}2]$ directions. Ir(332) was prepared by Ar^+ sputtering at 1 keV kinetic

*antonio.tejeda@u-psud.fr

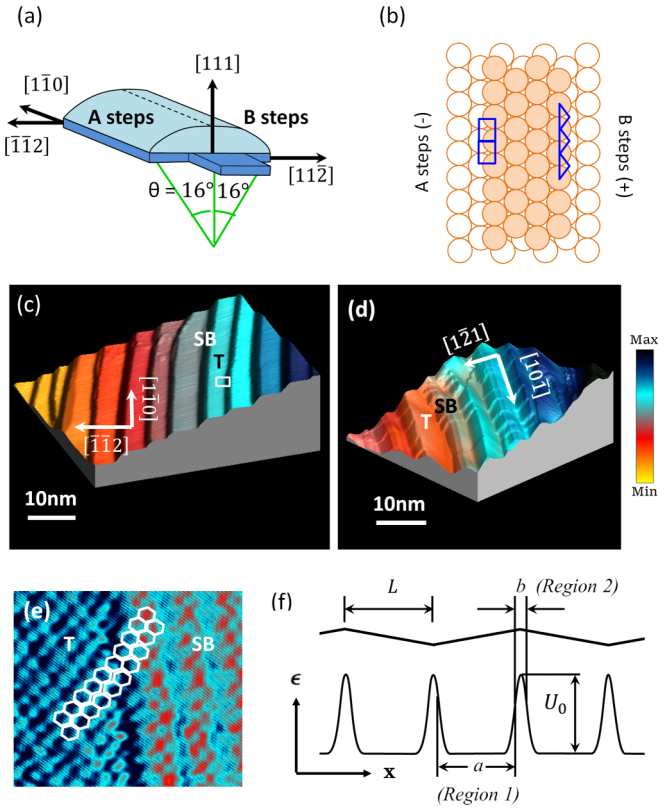

FIG. 1. (a) Scheme of a curved multivicinal Pt(111) crystal. (b) Step-edge structure of a noble metal with step edges running along the [10$\bar{1}$] direction. Step edges have square (triangular) atomic disposition in the A (B) step edges. (c) Three-dimensional representation of an STM image of graphene on the multivicinal Pt(111) crystal at a vicinal angle of ~ -7 deg and 3.5 ± 0.5 nm width facets (100 mV, 2.8 nA). The original surface relaxes into (111) terraces (T) and step bunching areas (SB). (d) STM image of graphene on Ir(332) (0.9 V, 0.5 nA). (e) Zoom on a T-SB boundary. The border width is of the order of the lattice parameter of graphene. Some hexagons are superimposed to indicate the continuity of graphene across the boundary. (f) Representation of the superperiodic structure (top) and energetic representation of the potential (bottom). L is the width of the T and SB regions, b is the varying potential region a few Å wide, and U_0 is the potential barrier.

energy followed by a short annealing at 920 K. Multivicinal Pt(111) crystal was prepared by four-step cycles consisting of Ar^+ sputtering at 1 keV, annealing at 970 K, Ar^+ sputtering at 1 keV, and annealing under oxygen atmosphere (1×10^{-7} mbar) for 10 min. A final flash at 1220 K ends the preparation. Graphene is grown by 10 min ethylene exposure to the substrate kept at 1070 K. This method is self-limited to 1 ML, as the growth needs the catalytic substrate to dissociate ethylene [34–36]. Dirac cones of the differently rotated moirés can be easily studied due to the angular resolution of photoemission.

III. RESULTS AND DISCUSSION

Figure 1 illustrates the one-dimensional nanostructured substrates for graphene growth. We have studied simultaneously graphene on different superperiodic potentials by using a multivicinal Pt(111) substrate [Figs. 1(a) and 1(c)] and Ir(332) [Figs. 1(d) and 1(e)]. The multivicinality of the curved substrate allows us to tune the spatial periodicity and to control the potential barrier depending on the facet width and the step-edge type. Figure 1(b) shows a scheme of the step-edge atomic structure at both sides of the (111) direction. A steps are characterized by a square disposition of edge atoms, while B-step atoms are arranged in a triangular fashion. The different atomic coordination at these step edges varies its reactivity.

When graphene is grown on the substrates, the original periodicity is modified due to faceting [33], so we have determined the spatial periodicity after growth by LEED and STM. Figure 1(c) shows an STM image of the multivicinal Pt(111) at -7° off normal, where a periodic arrangement of terraces (T) and step-bunching areas (SB) of similar width (3.5 ± 0.5 nm) is shown. Graphene grows like a carpet covering the steps, as appreciated in the STM images on Figs. 1(d) and 1(e). A sharp boundary between terraces and the step-bunching areas is appreciated. Graphene grown on these nanostructured substrates feels a one-dimensional potential varying at the T-SB boundaries, as illustrated in Fig. 1(f) and demonstrated in the following. The spatial extension of this potential is much smaller than the smooth potential in moiré structures where the mismatch between the atoms in the stacked layers varies progressively.

Any change in the graphene band structure induced by the periodic step potential should appear in photoemission measurements. It is therefore crucial to identify the direction where the potential varies, which can be determined from the isoenergetic cuts of the band structure. Figure 2(a) shows an isoenergetic cut at -330 meV. Different rotated Brillouin zones (indicated by dotted lines) appear due to the rotational domains of graphene. These domains correspond to graphene aligned with the substrate ($R0$ domain) or rotated by 25°, 30°, or 35° ($R25$, $R30$, and $R35$ domains, respectively). These domains are explicit in the isoenergetic cut due to the spectral weight arcs at the K points of the rotated Brillouin zones [Fig. 2(a)]. These arcs correspond to partially observed Dirac cones due to the photoemission matrix elements. These cones are sensitive to the one-dimensional potential along the direction perpendicular to the ΓK of Ir, so its effect is better observed on the $R0$ domain, which is far apart from spectral features from other rotated domains. Figures 2(b) and 2(c) show the band structure of this domain along ΓK and perpendicular to it. The $E(k)$ maps use a color scale proportional to the second derivative of the photoemission intensity. This representation allows us to observe faint spectral features even when bands are broad because of the step-width distribution on the substrate.

Figure 2(b) shows the dispersion along a direction perpendicular to ΓK through the K point, i.e., perpendicular to the step edges. The low dispersing spectral features at the Fermi level, ~ -1 and ~ -1.6 eV indicated by $S1$, $S2$, and I, correspond to substrate features [37,38]. Coexisting with them, the characteristic dispersion of graphene is observed. The Dirac point is above the Fermi level, as expected for graphene on noble metal [14,38–41], so a band-gap opening there is unobservable by photoemission. Strikingly, the spectral weight decreases below the Fermi level at two different reciprocal space locations when the electronic structure is proven perpendicular to the step edges [arrows in Fig. 2(b)]. On the contrary, the graphene dispersion is unaffected parallel to the step edges

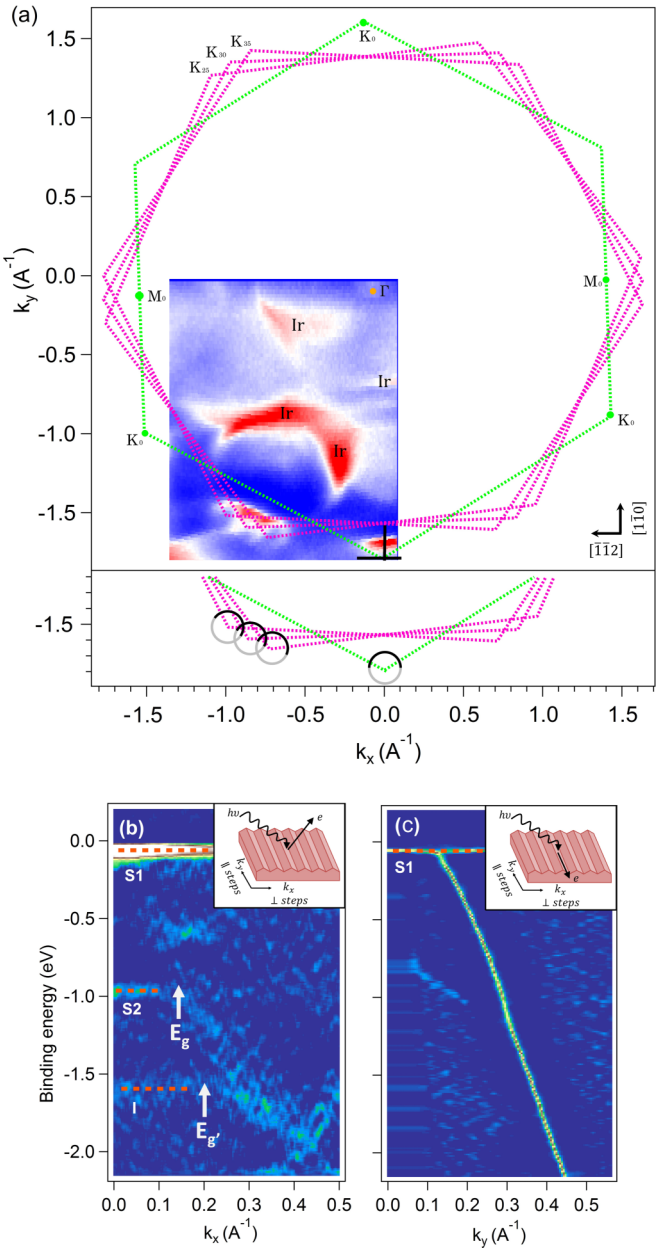

FIG. 2. Electronic structure of graphene on Ir(332). (a) Isoenergetic map of the band structure at −330 meV. The Brillouin zones associated with the different graphene rotations are shown by the dotted lines. "Ir" labels the substrate spectral features [38]. dI^2/d^2E maps of the dispersion relations $E(k)$ along the directions (b) perpendicular and (c) parallel to the steps [see the continuous lines in (a)]. The insets show the experimental geometry. $S1$, $S2$, and I are substrate-related features. The graphene dispersion exhibits minigaps of ∼400 meV (E_g) perpendicularly to the steps, while no band-gap opening is appreciated in the parallel direction.

[Fig. 2(c)], which indicates that the gap opening is related to the one-dimensional periodicity. The dispersion exhibits some slope changes, as previously observed [42,43]. Moreover, the k locations where the intensity decreases are compatible with a translation of the Dirac cone by multiples of $G = 2\pi/L$, where L is the one-dimensional structural periodicity. The one-dimensional surface potential has, therefore, opened

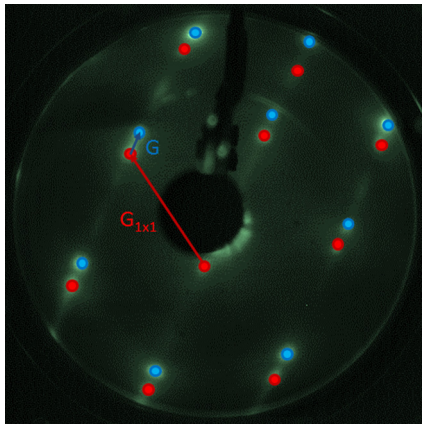

FIG. 3. LEED pattern of Ir(332) at 148 eV showing the $G_{1\times1}$ vector of the Ir(111) substrate and the G vector due to the facet periodicity. This G vector allows us to determine the spatial periodicity. In this case it is L = 1.8 ± 0.2 nm along the [1$\bar{2}$1] direction.

minigaps in graphene band structure. The spatial periodicity L can be obtained from STM images and from LEED. In LEED patterns, L is deduced from the distance between the (1 × 1) substrate spots and the replicas associated with the step-induced periodicity (Fig. 3).

The minigap opening is not exclusive of Ir(332). We have also determined the electronic structure in three different regions of a multivicinal Pt(111) single crystal [Figs. 4(a)–4(c)]. Minigaps appear in a reciprocal space position π/L away from the K point as shown in the second derivative images [Figs. 4(a) and 4(b)] as well as in the original spectra (Fig. 5). Spatial periodicities of $L = 3.2$ and 3.5 nm exhibit minigaps at different k locations [Figs. 4(a) and 4(b)]. The potential inducing the gap is different from the moiré potential existing in the nonvicinal surface [14], as the gap openings appear at different k in both cases (Fig. 6). Also, when the step-edge type varies from A to B [panels (b) and (c), respectively] and therefore the graphene is anchored differently to the substrate, the amplitude of the minigap varies. We thus conclude that the minigaps are correlated to the periodicity of the one-dimensional nanostructured substrate and also to its strength. The potential strength can be estimated by comparing the experimental data to the numerical solution of a Dirac Hamiltonian model [44–46]:

$$\cos(k_x L) = \cos(k_1 a)\cos(k_2 b) + \frac{k_y^2\hbar^2 v_f^2 - (V-E)^2}{\hbar^2 v_f^2 k_1 k_2}\sin(k_1 a)\sin(k_2 b) \quad (1)$$

with

$$k_1 = \left(\frac{[V-E]^2}{\hbar^2 v_f^2} - k_y^2\right)^{1/2} \quad (2)$$

$$k_2 = \left(\frac{[V-E]^2 - U_0^2}{\hbar^2 v_f^2} - k_y^2\right)^{1/2} \quad (3)$$

where v_f is the Fermi velocity and V describes the experimental doping of the system. The potential strength $U_0 b$

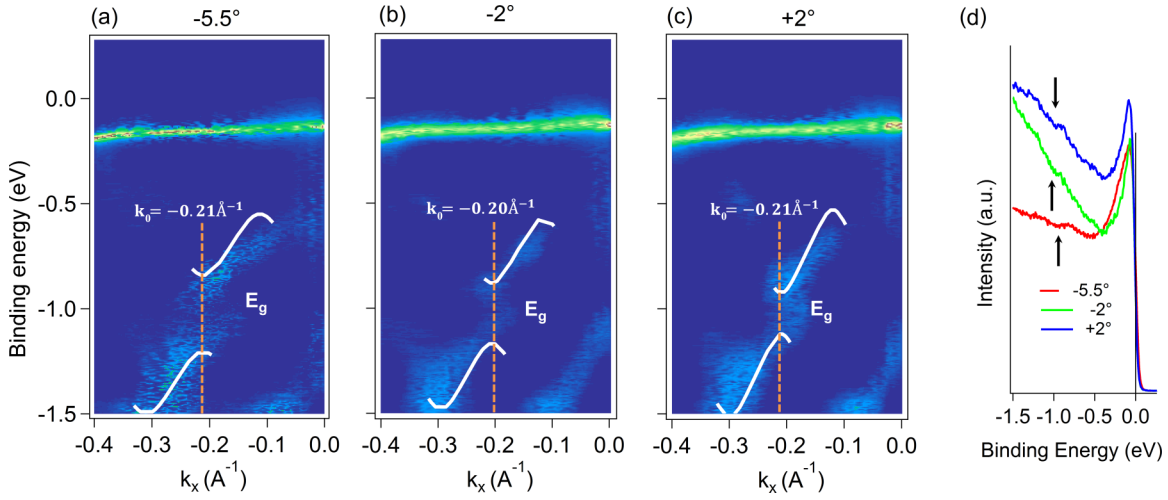

FIG. 4. Electronic structure of graphene on multivicinal Pt(111). dI^2/d^2E maps of the dispersion relations $E(k)$ for different facet size and orientation angle with respect to the (111) direction: (a) 3.2 ± 0.1 nm and -5.5°, (b) 3.5 ± 0.1 nm and -2°, and (c) 3.5 ± 0.1 nm and $+2^\circ$. The Dirac Hamiltonian model is shown as continuous lines, corresponding to a periodicity and potential strength of (a) 3.2 nm and 3.35 eV Å, (b) 3.5 nm and 2.8 eV Å, and (c) 3.5 nm and 1.8 eV Å. The vertical dashed lines indicate the k location of the band-gap opening (k_0). (d) Spectra of the original photoemission intensity around k_0, integrating in a k range of 0.1 Å^{-1}. Gaps are indicated by arrows. The Fermi level corresponds to 0 eV.

depends on the energy barrier U_0 and its spatial extent b [Fig. 1(f)]. By adjusting our experimental results with this model, we obtain for Ir(332) minigaps of 390 meV and a potential strength of 4.4 eV Å. For the different regions of the Pt(111) multivicinal substrate, the minigaps are explained for potential strengths of 3.2 eV Å [panel (a)], 2.8 eV Å [panel (b)], and 1.8 eV Å [panel (c)]. The $2\pi/L$ reciprocal vector determined by photoemission is in agreement with the structural periodicities observed by LEED and STM, which are $3.2 \pm 0.1, 3.5 \pm 0.1$, and 3.5 ± 0.1 nm, respectively. These results allow us to understand the observed minigaps promoted by the different step periodicities and different coupling to the substrate (Table I). In facets on the same material and with the same step edge but with different widths, a stronger potential barrier appears for smaller terrace widths, where the electronic confinement is enhanced. If we compare the graphene anchoring to the substrate in surfaces with A- and B-type step edges, we observe a doubling of the potential barrier for A steps, probably because of a higher graphene-substrate coupling. Finally, we observe that the Ir promotes higher

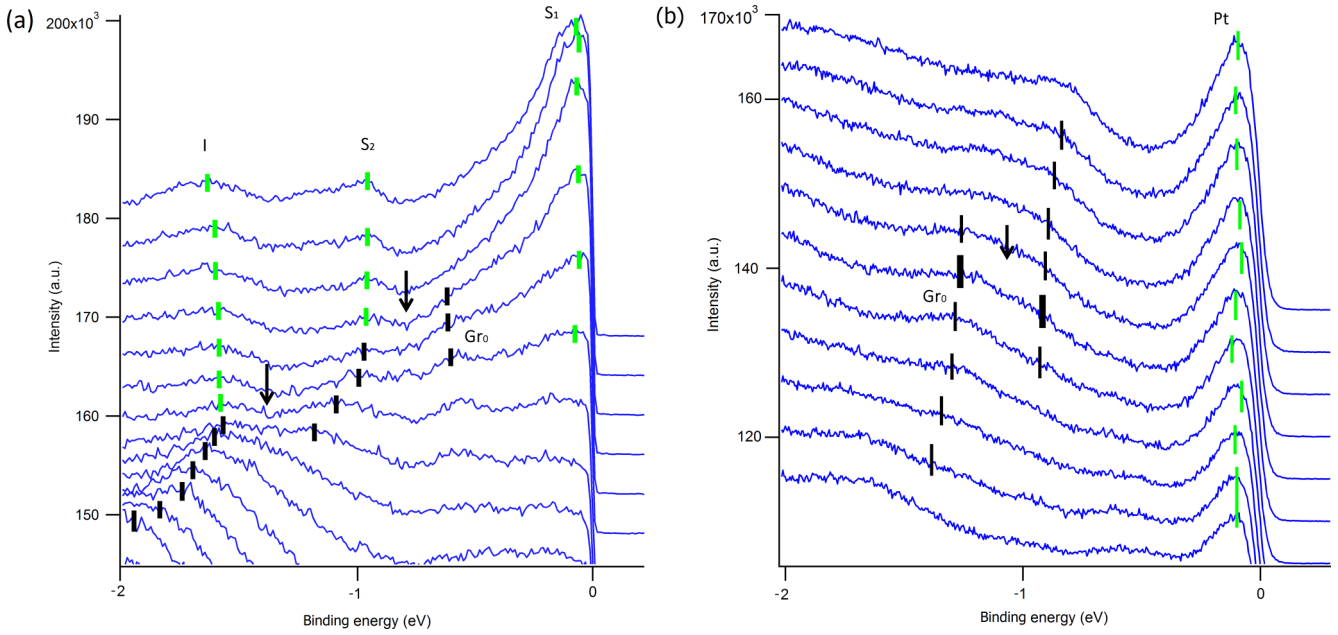

FIG. 5. Energy distribution curves of photoemission intensity. (a) EDCs for graphene on Ir(332). Black markers show the graphene dispersion and green markers show the iridium states I, $S1$, and $S2$. The arrows indicate the minigaps. (b) EDCs for graphene on multivicinal Pt corresponding to Fig. 3(c).

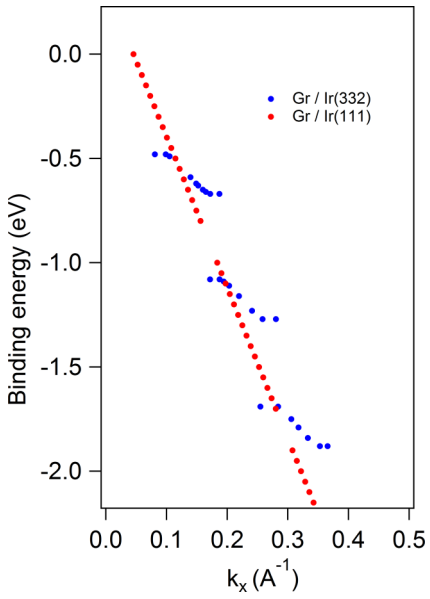

FIG. 6. Comparison between gap openings due to moiré and a one-dimensional periodicity. Simulation of gap openings in the one-dimensional periodicity of Fig. 2(a) (blue) and on the moiré of a Ir(111) surface (red). The minigaps due to Ir(111) moiré do not correspond to the gaps by nanostructuration as they appear at different k locations.

potential barriers because of the smaller graphene-substrate distance [47–49].

In all the previous situations, the physical origin of the gap is puzzling, since the Klein tunneling forbids the backscattering. However, the band gap can be understood by taking into account that Klein tunneling applies only for normal incidence to the potential barrier. As the system is a two-dimensional layer feeling a one-dimensional potential, Klein tunneling is not strict when electrons exhibit an out-of-normal incidence to the potential barrier. An alternative or supplementary origin to the band gap is the surface moiré. The moiré exists already on flat surfaces and promotes a band gap, which was attributed to a moiré-induced inequivalency between the A and B sublattices of graphene [14]. Vicinality may modify and amplify the moiré gap, possibly indicated by the presence of several Fourier components in the potential, associated with the vicinality and the moiré. The potential consists indeed of different Fourier components, as $E_g \sim E'_g$, whereas a single Fourier component potential should promote gaps of decreasing amplitude.

TABLE I. Gap opening in the studied materials and vicinalities.

Substrate	θ°	Terrace width (nm)	Step type	Gap (eV)
Pt multi.	−5.5	3.2	*A*	0.36
Pt multi.	−2	3.5	*A*	0.29
Pt multi.	+2	3.5	*B*	0.20
Ir (332)	+11	3.5	*B*	0.39

IV. SUMMARY

In conclusion, we have studied the effects of one-dimensional potentials on graphene by growing graphene on Ir(332) and on multivicinal Pt(111) substrates, demonstrating the band-gap tailoring in graphene band structure. Photoemission shows the presence of minigaps related to the spatial periodicity, whose strength can be varied with the step-edge type, the nature of the substrate, and in a more general way as a function of the anchoring of the graphene to the substrate. The minigap opening further demonstrates the presence of backward scattered electronic waves on the surface and the absence of Klein tunneling on the substrate, probably due to the fast-varying potential, of a spatial extent of the order of the lattice parameter of graphene. These results show a way to tailor graphene band structure in a solid-state system and possibly in analogous graphene metamaterials.

ACKNOWLEDGMENTS

We acknowledge the financial support of the Agence Nationale de la Recherche (France) under contract CoRiGraph. The authors acknowledge L. Brey for useful discussions and the support from F. Bertran and P. Le Fèvre and all the CASSIOPEE staff during ARPES beam time.

[1] M. F. Crommie, C. P. Lutz, and D. M. Eigler, Science **262**, 218 (1993).
[2] T.-C. Chiang, Surf. Sci. Rep. **39**, 181 (2000).
[3] R. Tsu, *Superlattice to Nanoelectronics* (Elsevier, Oxford, 2005).
[4] N. W. Ashcroft and N. D. Mermin, *Solid State Physics* (Brooks Cole, Orlando, 1976).
[5] A. Mugarza, A. Mascaraque, V. Pérez-Dieste, V. Repain, S. Rousset, F. J. García de Abajo, and J. E. Ortega, Phys. Rev. Lett. **87**, 107601 (2001).
[6] A. Mugarza and J. E. Ortega, J. Phys. Condens. Matter **15**, S3281 (2003).
[7] M. I. Katsnelson, K. S. Novoselov, and A. K. Geim, Nat. Phys. **2**, 620 (2006).
[8] A. F. Young and P. Kim, Nat. Phys. **5**, 222 (2009).
[9] N. Stander, B. Huard, and D. Goldhaber-Gordon, Phys. Rev. Lett. **102**, 026807 (2009).
[10] C.-H. Park, L. Yang, Y.-W. Son, M. L. Cohen, and S. G. Louie, Phys. Rev. Lett. **101**, 126804 (2008).
[11] C.-H. Park, L. Yang, Y.-W. Son, M. L. Cohen, and S. G. Louie, Nat. Phys. **4**, 213 (2008).
[12] J. Sun, H. A. Fertig, and L. Brey, Phys. Rev. Lett. **105**, 156801 (2010).
[13] A. L. Vázquez de Parga, F. Calleja, B. Borca, M. C. G. Passeggi Jr., J. J. Hinarejos, F. Guinea, and R. Miranda, Phys. Rev. Lett. **100**, 056807 (2008).
[14] I. Pletikosić, M. Kralj, P. Pervan, R. Brako, J. Coraux, A. T. N'Diaye, C. Busse, and T. Michely, Phys. Rev. Lett. **102**, 056808 (2009).
[15] M. N. Nair, I. Palacio, A. Celis, A. Zobelli, A. Gloter, S. Kubsky, J.-P. Turmaud, M. Conrad, C. Berger, W. de Heer, E. H. Conrad, A. Taleb-Ibrahimi, and A. Tejeda, Nano Lett. **17**, 2681 (2017).
[16] M. Conrad, F. Wang, M. Nevius, K. Jinkins, A. Celis, M. Narayanan-Nair, A. Taleb-Ibrahimi, A. Tejeda, Y. Garreau, A.

Vlad, A. Coati, P. F. Miceli, and E. H. Conrad, Nano Lett. **17**, 341 (2017).
[17] M. S. Nevius, M. Conrad, F. Wang, A. Celis, M. N. Nair, A. Taleb-Ibrahimi, A. Tejeda, and E. H. Conrad, Phys. Rev. Lett. **115**, 136802 (2015).
[18] M. Yankowitz, J. Xue, D. Cormode, J. D. Sanchez-Yamagishi, K. Watanabe, T. Taniguchi, P. Jarillo-Herrero, P. Jacquod, and B. J. LeRoy, Nat. Phys. **8**, 382 (2012).
[19] H. Yan, Z.-D. Chu, W. Yan, M. Liu, L. Meng, M. Yang, Y. Fan, J. Wang, R.-F. Dou, Y. Zhang, Z. Liu, J.-C. Nie, and L. He, Phys. Rev. B **87**, 075405 (2013).
[20] J.-K. Lee, S. Yamazaki, H. Yun, J. Park, G. P. Kennedy, G.-T. Kim, O. Pietzsch, R. Wiesendanger, S. W. Lee, S. Hong, U. Dettlaff-Weglikowska, and S. Roth, Nano Lett. **13**, 3494 (2013).
[21] J. C. Meyer, C. O. Girit, M. F. Crommie, and A. Zettl, Appl. Phys. Lett. **92**, 123110 (2008).
[22] C. Lin, X. Huang, F. Ke, C. Jin, N. Tong, X. Yin, L. Gan, X. Guo, R. Zhao, W. Yang, E. Wang, and Z. Hu, Phys. Rev. B **89**, 085416 (2014).
[23] M. Pisarra, D. Pacilé, P. Moras, P. M. Sheverdyaeva, A. Sindona, M. Papagno, and C. Carbone, Phys. Rev. B **89**, 195438 (2014).
[24] K. Nakatsuji, Y. Shibata, R. Niikura, F. Komori, K. Morita, and S. Tanaka, Phys. Rev. B **82**, 045428 (2010).
[25] T. Kajiwara, Y. Nakamori, A. Visikovskiy, T. Iimori, F. Komori, K. Nakatsuji, K. Mase, and S. Tanaka, Phys. Rev. B **87**, 121407 (2013).
[26] W.-J. Jang, M. W. Lee, H. Kim, S. Park, S. J. Jung, S. Lee, Y. J. Song, and S.-J. Kahng, J. Phys. Chem. C **119**, 19535 (2015).
[27] T. Ohta, J. T. Robinson, P. J. Feibelman, A. Bostwick, E. Rotenberg, and T. E. Beechem, Phys. Rev. Lett. **109**, 186807 (2012).
[28] L. Brey and H. A. Fertig, Phys. Rev. Lett. **103**, 046809 (2009).
[29] L. A. Ponomarenko, R. V. Gorbachev, G. L. Yu, D. C. Elias, R. Jalil, A. A. Patel, A. Mishchenko, A. S. Mayorov, C. R. Woods, J. R. Wallbank, M. Mucha-Kruczynski, B. A. Piot, M. Potemski, I. V. Grigorieva, K. S. Novoselov, F. Guinea, V. I. Fal'ko, and A. K. Geim, Nature (London) **497**, 594 (2013).
[30] B. Hunt, J. D. Sanchez-Yamagishi, A. F. Young, M. Yankowitz, B. J. LeRoy, K. Watanabe, T. Taniguchi, P. Moon, M. Koshino, P. Jarillo-Herrero, and R. C. Ashoori, Science **340**, 1427 (2013).
[31] G. L. Yu, R. V. Gorbachev, J. S. Tu, A. V. Kretinin, Y. Cao, R. Jalil, F. Withers, L. A. Ponomarenko, B. A. Piot, M. Potemski, D. C. Elias, X. Chen, K. Watanabe, T. Taniguchi, I. V. Grigorieva, K. S. Novoselov, V. I. Fal'ko, A. K. Geim, and A. Mishchenko, Nat. Phys. **10**, 525 (2014).
[32] C. R. Dean, L. Wang, P. Maher, C. Forsythe, F. Ghahari, Y. Gao, J. Katoch, M. Ishigami, P. Moon, M. Koshino, T. Taniguchi, K. Watanabe, K. L. Shepard, J. Hone, and P. Kim, Nature (London) **497**, 598 (2013).
[33] I. Šrut Rakić, M. Kralj, W. Jolie, P. Lazić, W. Sun, J. Ávila, M.-C. Asensio, F. Craes, V. M. Trontl, C. Busse, and P. Pervan, Carbon **110**, 267 (2016).
[34] A. T. N'Diaye, J. Coraux, T. N. Plasa, C. Busse, and T. Michely, New J. Phys. **10**, 043033 (2008).
[35] T. A. Land, T. Michely, R. J. Behm, J. C. Hemminger, and G. Comsa, Surf. Sci. **264**, 261 (1992).
[36] J. Coraux, A. T. N'Diaye, C. Busse, and T. Michely, Nano Lett. **8**, 565 (2008).
[37] I. Pletikosić, M. Kralj, D. Šokčević, R. Brako, P. Lazíc, and P. Pervan, J. Phys. Condens. Matter **22**, 135006 (2010).
[38] E. Starodub, A. Botswick, L. Moreschini, S. Nie, F. E. Gabaly, K. F. McCarty, and E. Rotenberg, Phys. Rev. B **83**, 125428 (2011).
[39] M. Kralj, I. Pletikosić, M. Petrovic, P. Pervan, M. Milun, A. T. N'Diaye, C. Busse, T. Michely, J. Fujii, and I. Vobornik, Phys. Rev. B **84**, 075427 (2011).
[40] M. Andersen, L. Hornekaer, and B. Hammer, Phys. Rev. B **90**, 155428 (2014).
[41] R. Larciprete, S. Ulstrup, P. Lacovig, M. Dalmiglio, M. Bianchi, F. Mazzola, L. Hornekaer, F. Orlando, A. Baraldi, P. Hofmann, and S. Lizzit, ACS Nano **6**, 9551 (2012).
[42] M. Bianchi, E. D. L. Rienks, S. Lizzit, A. Baraldi, R. Balog, L. Hornekær, and Ph. Hofmann, Phys. Rev. B **81**, 041403(R) (2010).
[43] A. Bostwick, T. Ohta, T. Seyller, K. Horn, and E. Rotenberg, Nat. Phys. **3**, 36 (2006).
[44] J. R. F. Lima, Phys. Lett. A **379**, 1372 (2015).
[45] J. R. F. Lima, Phys. Lett. A **379**, 179 (2015).
[46] N. M. R. Peres, J. Phys. Condens. Matter **21**, 095501 (2009).
[47] P. J. Feibelman, Phys. Rev. B **77**, 165419 (2008).
[48] A. T. N'Diaye, S. Bleikamp, P. J. Feibelman, and T. Michely, Phys. Rev. Lett. **97**, 215501 (2006).
[49] J. Wintterlin and M.-L. Bocquet, Surf. Sci. **603**, 1841 (2009).